POLITECNICO DI TORINO
Repository ISTITUZIONALE

Porous covalent organic nanotubes and their assembly in loops and toroids

Original
Porous covalent organic nanotubes and their assembly in loops and toroids / Koner, K., Karak, S., Kandambeth, S., Karak, S., Thomas, N., Leanza, L., Perego, C., Pesce, L., Capelli, R., Moun, M., Bhakar, M., Ajithkumar, T.G., Pavan, G.M., Banerjee, R.. - In: NATURE CHEMISTRY. - ISSN 1755-4330. - ELETTRONICO. - (2022). [10.1038/s41557-022-00908-1]

Availability:
This version is available at: 11583/2959635 since: 2022-03-26T09:56:28Z

Publisher:
Nature

Published
DOI:10.1038/s41557-022-00908-1

Terms of use:

This article is made available under terms and conditions as specified in the corresponding bibliographic description in the repository

Publisher copyright
GENERICO -- per es. Nature : semplice rinvio dal preprint/submitted, o postprint/AAM [ex default]

The original publication is available at https://www.nature.com/articles/s41557-022-00908-1 / http://dx.doi.org/10.1038/s41557-022-00908-1.

(Article begins on next page)

16 June 2026

1. Supplementary Information:

A. Flat Files

Item	**Present?**	**Filename** **This should be the name the file is saved as when it is uploaded to our system, and should include the file extension. The extension must be .pdf**	**A brief, numerical description of file contents.** **i.e.: *Supplementary Figures 1-4, Supplementary Discussion, and Supplementary Tables 1-4.***
Supplementary Information	Yes	NEW_Supplementary Information.pdf	Supplementary Figures 1-41, Supplementary Discussion, and Supplementary Tables 1-2

B. Additional Supplementary Files

Type	**Number** **If there are multiple files of the same type this should be the numerical indicator. i.e. "1" for Video 1, "2" for Video 2, etc.**	**Filename** **This should be the name the file is saved as when it is uploaded to our system, and should include the file extension. i.e.: *Smith_ Supplementary_Video_1. mov***	**Legend or Descriptive Caption** **Describe the contents of the file**
Supplementary Video	1	Banerjee_video_1.avi	Coarse-Grained model for intertwine CONT-1
Supplementary Video	2	Banerjee_video_2.avi	Model for CONT-1 in DCM
Supplementary Video	3	Banerjee_video_3.avi	Model for CONT-1 in water
Supplementary Video	4	Banerjee_video_4.avi	Zoomed video of CONT-1 in DCM
Supplementary Video	5	Banerjee_video_5.avi	Zoomed video of CONT-1 in water
Supplementary Data	1	Supp Data 1: Source Data Supplementary Fig 12.xls	Source Data for Supplementary figure 12: Pore size distribution of CONT-1 from N_2 adsorption isotherm.
Supplementary Data	2	Supp Data 2: Source Data Supplementary Fig 26.xls	Source Data for Supplementary figure 26: DLS study for

			toroids
Supplementary Data	3	Supp Data 3: Source Data Supplementary Fig 31.xls	Source Data for Supplementary figure 31: Calculation of yield of toroids

2. Source Data

Parent Figure or Table	**Filename** **This should be the name the file is saved as when it is uploaded to our system, and should include the file extension. i.e.: *Smith_SourceData_Fig1.xls,* or *Smith_ Unmodified_Gels_Fig1.pdf***	**Data description** **i.e.: Unprocessed Western Blots and/or gels, Statistical Source Data, etc.**
Source Data Fig. 2	Source Data Fig 2.xls	The Excel sheet contains FTIR data, solid state ^{13}C NMR, solid state ^{13}C HPDEC NMR, N_2 adsorption isotherm and pore size distribution of CONT-1.
Source Data Fig. 4	Source Data Fig 4.xls	N_2 adsorption isotherm of pristine CONT-1 and CONT-1 after water treatment (immersed in water) for 7 days
Source Data Fig. 5	Source Data Fig 5.xls	Angle 1 and Angle 2 distribution for CONT-1 in DCM, THF, water and Vacuum.
Source Data Fig. 6	Source Data Fig 6.xls	DLS data for toroids and histogram plot for radius of toroids from SEM images

Porous covalent organic nanotubes and their assembly in loops and toroids

Kalipada Koner,[1,2] Shayan Karak,[1,2] Sharath Kandambeth,[3] Suvendu Karak,[3*] Neethu Thomas,[3] Luigi Leanza,[4] Claudio Perego,[5] Luca Pesce,[5] Riccardo Capelli,[4] Monika Moun,[6] Monika Bhakar,[6] Thalasseril G. Ajithkumar,[3] Giovanni M. Pavan,[4,5*] and Rahul Banerjee[1,2*]

[1]Department of Chemical Sciences, Indian Institute of Science Education and Research, Kolkata, Mohanpur, 741246, India.

[2]Centre for Advanced Functional Materials, Indian Institute of Science Education and Research, Kolkata, Mohanpur,741246, India.

[3]Central NMR Facility and Physical/Materials Chemistry Division, CSIR-National Chemical Laboratory, Dr. Homi Bhabha Road, Pune 411008, India.

[4] Department of Applied Science and Technology, Politecnico di Torino, Torino 10129, Italy.

[5]Department of Innovative Technologies, University of Applied Sciences and Arts of Southern Switzerland, Viganello-Lugano CH-6962, Switzerland.

[6]Department of Physical Sciences, Indian Institute of Science Education and Research (IISER) Mohali, Sector 81, S. A. S. Nagar, Manauli, 140306, India.

Abstract

Carbon nanotubes, and synthetic organic nanotubes more generally, have been explored in many applications in electronic devices, energy storage, catalysis, and biosensors over past decade. Despite noteworthy progress made in the synthesis of nanotubular architectures with well-defined lengths and diameter, purely covalent bonded organic nanotubes have remained somewhat challenging to prepare. Here, we report the synthesis of covalent bonded porous organic nanotubes (CONTs) by Schiff base reaction between a tetratopic amine-functionalized triptycene and a linear dialdehyde. The spatial orientation of the functional groups promotes the growth of the framework in one-dimension, and the strong covalent bonds between C, N, and O impart the resulting CONTs with high thermal and chemical stability. Upon ultrasonication, the CONTs form intertwined structures that go on to coil and form toroidal superstructures. Computational studies give some insight into the effect of the solvent in this assembly process.

Main Text:

In the construction of reticular frameworks of any dimension the geometry and bonding capability of the building units, as well as the self-correction capability of the reversible linkages between them, are crucial aspects.[1,2] Through dynamic covalent chemistry, a wide

variety of organic cages (zero-dimensional) as well as two- and three-dimensional covalent organic frameworks (COFs) have been synthesized.[3-6] However, controlling the periodic arrangement of covalent bonds in extended one-dimensional solids is still in infancy. Nanotubes are one group of such covalent bonded structures where limited synthetic approaches have been developed.[7,8] These one-dimensional hollow tubular nanostructures are attractive for applications in electronic devices, energy storage, catalysis, membrane separation, and biosensors.[9-11] Carbon nanotubes (CNTs) are the most explored members of this family due to their electronic and mechanical properties. They are generally synthesized by rolling two-dimensional graphite sheets around the edges following various methods such as arc discharge, electrolysis, chemical vapor deposition (CVD), plasma torch, and hydrothermal techniques.[12-18] These methods demand harsh reaction conditions and high temperature. Furthermore, the incorporation of pre-designed functionalities is difficult due to the CNTs' insolubility in common organic solvents.

Although self-assembly and disassembly have been shown to lead to such nanotubular architectures,[19-21] it has remained challenging to control their size on the nanoscale, as well as their morphology and composition. One of the main challenges in the bottom-up synthesis of such self-assembled nanostructures is the need to simultaneously control their structure and their morphology. In particular, a variation in composition of the building blocks can alter the system's nanoscopic assembly and in turn the overall morphology of the resulting structures — making the systematic tuning of their size or shape difficult.[22,23] The supramolecular strategy also often leads to significant structural alterations during functionalization, as functional groups alter the interactions between the building blocks.

Herein, we present the synthesis of covalent bonded porous organic nanotubes, using organic building blocks designed to assemble into one-dimensional covalent organic nanotubes

(CONTs) through dynamic covalent chemistry. A tetratopic triptycene derivative with a dihedral angle of ~120º was combined with linear ditopic ligands by a reversible Schiff base reaction, leading to the formation of CONTs. The formation of either the thermodynamically or the kinetically stable product was favoured by adjusting the reaction conditions. The reversibility of the Schiff base reaction imparts error-correction capability to the system, which under thermodynamic control allowed the selective formation of the ordered porous covalent 1D tubular framework over a random polymeric structure. Due to the high strength and stability of the covalent bonds, the synthesized CONTs display excellent chemical and thermal stability. These extended nanotubes (up to several microns in length) with sub-nanometer diameter exhibit porosity as high as 321 m^2g^{-1}. This one-pot reaction strategy of CONT synthesis may also be suitable for large-scale synthesis.

A time-dependent electron microscopic study into the morphological evolution of these CONTs showed that the isolated tubular morphologies go on to form intertwined toroidal structures.

Results and Discussion

Design and synthesis of CONTs: We have focused on a tetratopic tetraamine and a linear dialdehyde to construct the nanotubular covalent organic architecture (Fig. 1). The tetraaminotriptycene (TAT) features two opposite terminal amine pairs at a dihedral angle of ~120º (Fig. 1b), and it is this orientation of amine functionalities in the TAT units that promotes the formation of covalent linkages in one dimension. The building blocks (Fig. 1b) were chosen for their geometry and energy optimization, which on aldehyde–amine condensation favour the formation of two geminal imine bonds that are trans to each other. This in turn ensures the framework's formation in one dimension, as the non-functionalized benzene rings are kept towards the inner wall of the resulting nanotube.

To check the reaction's feasibility, we first synthesized a monomeric unit by reacting the TAT with *2*-methoxy benzaldehyde **(MB)**. High-resolution mass spectrometry (HRMS) analysis indicates that the stoichiometric condensation of TAT and *2*-methoxy benzaldehyde results in a mixture of three products. These products are monomer-**1** (diimidazole-triptycene); with two imidazole rings, monomer-**2** (diimine-monoimidazole-triptycene); with one imidazole ring and two imine bonds; and monomer-**3** (tetraimine-triptycene); with four imine bonds (Supplementary Section 2). By carefully examining the monomers, we concluded that imidazole formation is the competitive reaction preventing the nanotube formation. Thus, imine bond formation was optimized to reduce the imidazole formation with sequential modifications of the synthetic conditions (Supplementary Table 1, Supplementary Figures 3-8).

We then synthesized two CONTs (CONT-1 & CONT-2) *via* imine condensation reactions by combining a mixture of one equivalent of TAT (15.7 mg, 0.05 mmol) and two equivalents of either *2,5*-dimethoxybenzene-*1,4*-dicarboxaldehyde (DMDA) (19.4 mg, 0.1 mmol) for CONT-1 or terephthalaldehyde (TA) (13.4 mg, 0.1 mmol) for CONT-2. The dropwise addition of amine solution in dichloromethane (DCM) into the aldehyde solution (in DCM) in the presence of 0.5 mL 6 (M) acetic acid results in the cloudy precipitate (Supplementary Section 1). The resulting precipitate was collected by centrifugation followed by washing with anhydrous THF and then evacuated at 120 °C for 12 hours to yield 25.05 mg of CONT-1 and 13.3 mg of CONT-2 [78%, and 51% yield of CONT-1 and CONT-2 respectively based on TAT] as off-white solid.

Structural characterization : The FTIR spectra of both CONTs show the characteristic peaks at 1610 cm^{-1}, which are characteristic -C=N- stretching modes for imine bonds (Fig. 2a, Supplementary Figure 9). Solid-state Cross-Polarization Magic angle Spinning (CPMAS) NMR spectroscopy of the ^{13}C and ^{15}N nuclei was performed to validate the formation,

connectivity, and atomic level construction of the CONT-1 backbone (Fig. 2b, Supplementary Figure 10). Solid-state ^{13}C CP-MAS NMR spectroscopy shows the characteristic peaks of the imine (−C=N−) bonded carbon atoms at 155.5 ppm, whereas the methyl carbon appears at 53.5 ppm. The NMR spectrum also displayed discrete resonances in the aromatic region between 150 and 110.5 ppm (Fig. 2b). Solid-state High-Power Decoupled (HPDEC) ^{13}C spectrum quantifies the number of different carbon atoms in the tube backbone. According to the reaction scheme, the basic unit consists of 20 carbons from TAT and 40 carbons from DMDA. Out of these, 18 carbons from TAT and 32 carbons from DMDA appear in the aromatic and carbonyl region (200 to 100 ppm), two carbons of TAT and eight carbons of DMDA appear in the aliphatic region (~55 ppm) (Fig. 2c). Thus, one would expect an aromatic to the aliphatic carbon ratio of 5:1 for a complete reaction. The ratio obtained from the ^{13}C HPDEC spectrum is close to 5:1. The peak at 186 ppm was assigned as free aldehyde functionality generated from the defect sites at the nanotube surface (Supplementary Figure 10). Although the optimized condition for the model system results in no imidazole formation, the nanotube contains a meager percentage (6-8%) of aldehyde moieties as defects in the framework. We have recorded multiple solid-state HPDEC ^{13}C NMR spectra with different synthetic scales (yielding 150 mg and 280 mg of CONT-1) in two different instruments to quantify the defect in CONT-1. All the spectra are consistent to show 6-8% defect in the nanotube framework (Supplementary Section 4). The ^{15}N CP-MAS spectrum of CONT-1 displayed two discrete peaks, a resonance at 240 ppm and another at 148 ppm, indicating two distinct nitrogen sites. The characteristic peak at 240 ppm suggests the formation of the imine (−C=N−) bonded nitrogen atoms. The resonance at 148 ppm indicates the presence of N–H group, which may be due to imidazole ring formation at the defect sites (Supplementary Section 16). Thermogravimetric analysis (TGA) of the activated CONT-1 under N_2 atmosphere indicates that the framework has thermal stability up to 400º

C, and there is no guest molecule inside the nanotubes (Supplementary Figure 34). The porosity of the CONTs was evaluated by measuring N_2 adsorption isotherm at 77K (Fig. 2d, Supplementary Figure 11). Activated CONTs (after degassing at 140 ºC for 10 hours) showed reversible type II N_2 adsorption isotherm. The BET surface areas of the activated CONT-1 and -2 were 321 m^2g^{-1} and 52 m^2g^{-1}, respectively (Supplementary Figure 11). The pore size distribution of both the CONTs was calculated based on the nonlocal density functional theory (NLDFT) (Fig. 2d and Supplementary Figure 12). The pore size distribution, which indicates two types of pores of 1-2 nm and 3.5-4.5 nm of size, is in good agreement with the theoretically predicted structure (Supplementary Figure 12). The 3.5-4.5 nm pore distribution refers to the main hollow tubular channels running along the length of the CONTs. The 1-2 nm pore distribution corresponds to the side pores located on the nanotubes' walls.

Morphology of nanotubes: Scanning Electron Microscopy (SEM) images of CONTs reveal uniform tubular morphology, with an average diameter of ~5 nm (Supplementary Figure 13). High-Resolution Transmission Electron microscopy (HRTEM) (Fig. 2e) identifies the hollow tubular nature at the interior with a constant diameter of ~5 nm throughout the entire length of the nanotube (Supplementary Figure 14). Atomic Force Microscopy (AFM) further corroborates this finding (Supplementary Figure 15). The AFM height profile shows the uniform diameter of ~5 nm of the single nanotube, which is in good conjunction with the TEM results and nanotubes' theoretically predicted structure (Fig. 2f). Additionally, electronic microscopic images show that the single-walled CONTs are intertwined, which might be due to their high length to width ratio (~avg. 300:1). The microscopic analysis further confirms that the individual units of the intertwined nanotubes' diameter having a close match (~5 nm) with isolated single nanotubes (Supplementary Figure 15). We have isolated the reaction mixtures at different time intervals and characterized them *via* SEM analysis to shed more light on the CONT-1 formation (Supplementary Figure 16). CONT-1

formation starts within 6 hours of reaction. These CONTs are 100-200 nm in length and ~5 nm in diameter. After 12 hours, the CONTs grow up to 500-800 nm in length with a diameter of ~5 nm (avg. length to diameter ratio 130:1). The intertwining starts after 24-30 hours when the length to diameter ratio of the CONTs increases significantly (~avg. 200:1).

The rapid increase in the length of CONTs induces high flexibility, promoting intertwined structures. After 36 hours of reaction, almost all CONTs become completely intertwined, and no significant morphological changes are observed (Supplementary Figure 16). We speculate that the defect centers could trigger this intertwining (Fig. 3). After 6 hours, two nanotubes uniformly intertwine, following a particular pattern where the twining pitch is 70 (±10) nm (Supplementary Figures 19, 20). The resulting intertwined nanotube thread again entangles with the available mesh of CONTs. The width of intertwined nanotubes reaches up to ~100 nm (maximum) with time (Supplementary Figures 16, 17, and 18). However, the intertwining pitch remains constant (~70 nm) irrespective of their size and diameter.

Stability of CONTs: To our surprise, the nanotubes retain their morphology in a broad range of solvents of various polarities (Figs. 4a, b). The N_2 adsorption isotherm confirms the structural stability in water after seven days (Fig. 4d). We drop-casted the well-dispersed CONTs on a silicon wafer and heated it at different temperatures to validate the material's temperature stability. The morphology remained unaltered even at 150 ºC (Fig. 4c). However, the width of intertwined CONT-1 varied with the solvents' nature, as the solvent environment seems to impact the interaction among CONTs.

Theoretical investigation of the self-assembly: To obtain a deeper insight into the molecular factors that drive the CONT self-assembly in different solvents, we used multiscale molecular models to simulate the CONTs in different solvent conditions. Following well-established approaches [24,25], we developed an all-atom (AA) model of CONT-1 composed of 15 TAT layers (Fig. 5a). This AA model was immersed in explicit DCM or THF solvent (Fig.

4b) and equilibrated *via* 200 ns of molecular dynamics (AA-MD) at T=20 °C (Supplementary Section 26). For comparison, we also equilibrated this CONT-1 model in water and in the gas phase (i.e., absence of solvent). The AA-MD simulations showed that in DCM and THF the CONT-1 equilibrates to configurations slightly deviating from the initial perfect one (Fig. 5b), as also demonstrated by the distributions of angles 1 and 2 (Fig. 5c). On the contrary, in water, the tubules tend to compress along the longitudinal axis due to strong solvophobic effects (Figs. 5b, c, see also Supplementary Section 26). A similar structural compression is also seen in the gas phase. In all cases, the diameter of the AA CONT models remains compatible with that estimated experimentally (see Figs. 4a, b). We then used these AA models as a guideline to develop a minimalistic Coarse-Grained (CG) model[26] that, while more approximated, allowed us to study the behavior and interactions between the CONTs on a higher scale. In this CG model, each TAT unit in the CONT-1 structure is represented by a single CG particle, interconnected with the other neighbor TAT particles *via* harmonic bonds (Fig. 5d). The CG particles interact with each other *via* a simple Lennard-Jones (LJ) potential. The parameters of this CG model were initially optimized to obtain a behavior consistent with that of the AA CONT-1 model in explicit DCM solvent (Supplementary Section 26.2). This allowed us to simulate with reasonable accuracy the behavior of long CONT models composed of 500 TAT layers (Fig. 5c: tubule length ~820 nm). Starting from a system configuration with two separated, initially parallel tubes, we ran CG-MD simulations in which the depth of the LJ potential (ε) acting between the CG beads was systematically varied, modulating the nanotube-nanotube interaction as to model a change of solvent in the system (ε sets the strength of the non-bonded interaction between the CG particles of the CONTs: see SI for details). Comparison with the AA models allowed us to relate the stronger/weaker CONT-CONT interactions in the CG models to the effect of increased/decreased solvophobicity of the tubules in different realistic solvent conditions. For

ε values <1 kJ mol^{-1}, the two CONTs interacted only weakly and intermittently, and no intertwining was observed during the CG-MD (weak solvophobicity). Instead, for ε≥1 kJ mol^{-1}, we observed persistent interactions and intertwining of the two CONTs. As indicated by umbrella sampling[27] calculations (Supplementary Section 26), ε values in the CG models of 2 and 2.5 kJ mol^{-1} provided a CONT-CONT interaction respectively compatible with that obtained with the AA models in explicit DCM and THF solvents (Supplementary Figure 38). In these cases (Figs. 5e-f), the CG-MD showed an average intertwining pitch consistent with that observed experimentally (~70±10 nm). These results also demonstrated that the interactions between the CONTs in water (stronger solvophobic effects) or in the gas-phase are compatible with higher ε values in the CG model. However, at ε>2.5 kJ mol^{-1}, the formation of well-defined helices becomes less favored, and the CONTs tend to interact further, generating tighter and less-defined hierarchical assemblies. In general, these CG-MD results indicate that the combination of solvophobic effects with the geometric structure and flexibility of the CONTs is a determinant factor controlling the intertwining observed experimentally.

Formation of toroids: The intertwined CONTs further self-assemble to form a toroidal superstructure upon ultrasonication (Figs. 6a-c).[28-30] We have observed that tetrahydrofuran (THF) is the best solvent to obtain the toroids in high yields (up to 60%) (Supplementary Figure 31). Toroidal micro ring formation also proceeds in other solvents like o-xylene and o-dichlorobenzene (DCB), with a yield of <5%. The toroids are purified from the mixture of intertwined nanotubes by filtering through a Whatman 42 filter paper (pore size of 2.5 μm) (Supplementary Section 17). The Dynamic Light Scattering (DLS) study of the filtrate provides the average outer diameter of 600 nm at 20 ºC with a polydispersity index less than 0.15 (Fig. 6d). FESEM images show that the toroid diameters range from 300 nm to 900 nm (Fig. 6f). However, the rings' thickness remains constant (~50 nm) around their

circumference (Supplementary Figure 27, 28). Topographical analysis using AFM further confirms the same toroidal morphology (Supplementary Figure 29). HRTEM images of toroids prove that the walls of toroids are composed of intertwined hollow nanotubes with a ~5 nm individual tube diameter and a constant pitch of ~70 nm (Supplementary Figure 28). Detailed SEM, TEM, and AFM analyses reveal that the intertwined nanotubes first bend to form non-uniform loops (diameter 100-1000 nm) (Fig. 6f). The most probable mechanism involves the creation of bubbles in THF.[31] We propose that the bubbles would act as the template for hydrophobic CONTs, which would eventually orient themselves around the bubbles' circumference. Being bent at the bubble–THF interface, nanotubes would form loops when the bubble collapses (Supplementary Figure 30). The untied intertwined nanotubes would then coil up in both the transverse and longitudinal directions to create a closed and coiled loop-like structure of various diameters (0.1-1 μm). These spiral loop structures were later transformed into toroidal structures (Fig. 6f).

Conclusion

In summary, we have designed covalently connected and porous single-walled covalent organic nanotubes (CONTs). The efficient synthetic protocol results in porous nanotubes with high chemical and thermal stability, that we anticipate will be amenable to functionalization. The nanotubes then further assemble into a toroidal superstructure. Our proposed mechanism involves the intertwining of the nanotubes, which then coil up to construct toroidal superstructures under the influence of solvent and mechanical stimuli. The toroids were separated from intertwined nanotubes by their size distribution. The main characteristic features of CONTs, including their flexibility, capacity to intertwin and form toroids, are similar to those of CNTs. We hope that this work will lead to the synthesis and functionalization of other organic nanotubes with high chemical and thermal stability, which

could facilitate their exploration for application in fields such as catalysis, electrochemistry or biochemistry.

Acknowledgment

K.K. acknowledges UGC for a senior research fellowship (SRF), and Sh.K. acknowledges IISER Kolkata for the Integrated Ph.D. fellowship. R. B. acknowledges the funding from the DST-Swarna Jayanti Fellowship grant (DST/SJF/CSA-02/2016-2017), DST Mission Innovation [DST/TM/EWO/MI/CCUS/17 and DST/TMD(EWO)/IC5-2018/01(C)] and DST SERB [CRG/2018/000314] for funding. G.M.P. acknowledges the funding received by the Swiss National Science Foundation (SNSF grants IZLIZ2_183336) and by the European Research Council (ERC) under the European' 'Union's Horizon 2020 research and innovation program (grant agreement no. 818776 – DYNAPOL). We acknowledge Goutam Sheet for collecting the AFM data and Dr. P. R. Rajamohanan for discussion about NMR results. G.M.P, L.L., C.C, R.C., and L.P. also acknowledge the computational resources provided by the Swiss National Supercomputing Center (CSCS) and by CINECA. We thank Charly Empereur-mot and Annalisa Cardellini for the useful discussions. M.M. and M.B. acknowledges DST-Swarna Jayanti Fellowship grant (DST/SJF/PSA01/2015-16).

AUTHOR INFORMATION

Corresponding Authors

r.banerjee@iiserkol.ac.in

suvkarak@gmail.com

giovanni.pavan@polito.it

Contributions

Designing and choosing building blocks have been made by KK, SK, and RB. KK and ShK synthesized all the materials. SEM, TEM and AFM performed by KK. SSNMR was done by

NT and TGA. AFM images in Fig. 1 and Supplementary Figure 15 were collected by MM and MB. The nanotube architecture was constructed by SK. Theoretical calculation of intertwining and solvents' role was done by CP, LL, LP, RC, and GMP. All experiments were planned by KK, SK, SuK, and RB. RB supervised the whole project. KK, SK, SuK, and RB analyzed all the results and co-wrote the manuscript taking inputs from all co-authors.

Competing interests

The authors declare no competing financial interests.

Figure Captions

Fig. 1 | Design and synthesis of covalent organic nanotubes: a) Schematic representation of the synthesis of cages (0D), 1D (CONTs), 2D and 3D COFs based on the reversible aldehyde–amine condensation. **b)** Structures of the porous CONTs synthesized from a tetra(amine)-functionalized triptycene (TAT) and one of linear dialdehydes, DMDA and TA. **c** Schematic representation of the resulting CONTs (left, front and right, side view).

Fig. 2 | Characterization of nanotubes: a) FTIR spectra of TAT, DMDA, and CONT-1. **b)** ^{13}C Solid-state CP-MAS NMR spectrum of the CONT-1. **c)** Solid-state High-Power Decoupled (HPDEC) ^{13}C NMR spectrum of the CONT-1 for quantitative analysis of carbonyl group. **d)** N_2 adsorption isotherm at 77 K of CONT-1. The NLDFT pore size distribution from the N_2 adsorption analysis (inset) shows the micro (1.2-2.0 nm) and mesoporous (3.5 nm) nature of the nanotubes. **e)** TEM image of isolated single nanotubes. Inset shows the hollow interior of ~5 nm of CONT-1 — this is a zoomed portion from another CONT. **f)** AFM image of a single nanotube, showing the nanotube length of ~4.5μm. Height profile indicates a uniform diameter of 5 nm.

Fig. 3 | Intertwining of the CONTs: (a) Graphical representation of the increasing intertwining of the nantobues, from top to middle to bottom. (b-d) Characterization by HRTEM (b) SEM (c) and AFM of each of the situations represented in panel (a) (d) shows two flexible CONTs interconnect first at a single point. This interconnection leads to the formation of intertwined structures with a characteristic average pitch. This in turn generates the assemblies shown on panel d, bottom.

Fig. 4 | Stability of CONT-1: a) TEM and **b)** SEM images of CONT-1 immersed in water, acetonitrile, o-DCB and o-xylene(the dielectric constants are mentioned in the bracket) for 7 days indicate its solvent stability. **c)** SEM images of CONT-1 before and after heat treatment at 150º C show the tube's high thermal stability. **d)** N_2 adsorption isotherm of CONT-1 before and after water treatment (immersed in water) for seven days.

Fig. 5 | Multiscale molecular models of the CONT-1 system. a) AA model of CONT-1. The two characteristic angles (Angles 1 and 2) formed by the TAT moieties in the CONT structure are highlighted in orange and green colours. **b)** MD snapshots of the AA model of the initially perfect CONT-1 (left) and the equilibrated CONT-1 tube (after 200 ns of AA-MD) in different solvents: in

DCM, THF, vacuum (VAC), and in water (WAT). **c)** Distributions of the angles 1 and 2 in the structure of the equilibrated CONT-1 computed along the AA-MD in the different environments. Black lines indicate the value of angles 1 and 2 in the initially perfect conformation of the tube, the peaks of the colored distributions indicate the most probable values for the angles in the various solvents. **d)** Mapping of the AA structure of the model into the CG CONT model (interconnected red CG beads). **e)** Spontaneous intertwining of two CONTs during CG-MD simulations. Starting from initially parallel CONTs (left), different average intertwining pitches are obtained during the CG-MD as a function of the interaction strength (ε) between the CG beads (simulation time is expressed in CG-MD integration time steps units, τ). **f)** Average intertwining pitch as a function of CG-MD simulation time, measured for different values of ε (values of ε of 2-2.5 correspond to the CONT-CONT interaction in DCM and THF, respectively.

Fig. 6 | Characterization of toroidal structures. a) Schematic representation of toroids. **b,c)** SEM (b) and AFM (c) images of toroids, respectively. **d)** DLS study of the toroids after separating them from the nanotubes. Inset indicates a histogram of contour length of rings measured directly from SEM images. **e,f)** Schematic illustration (e) and characterization by SEM (f) of intertwined nanotubes that gradually form toroidal architectures.

References

1. Liu, Y., O'Keeffe, M., Treacy, M. M. J. & Yaghi, O. M. The geometry of periodic knots, polycatenanes and weaving from a chemical perspective: a library for reticular chemistry. *Chem. Soc. Rev.* **47**, 4642 (2018).
2. Zhang, B. et al. Reticular Synthesis of Multinary Covalent Organic Frameworks. *J. Am. Chem. Soc.* **141**, 11420–11424 (2019).
3. Tozawa, T. et al. Porous organic cages. *Nat. Mater.* **8**, 973-978 (2009).
4. Côte, A. P. et al. Porous, Crystalline, Covalent Organic Frameworks. *Science* **310**, 1166-1170 (2005).
5. Liu, Y. et al. Weaving of organic threads into a crystalline covalent organic framework. *Science* **351**, 365-369 (2016).
6. Uribe-Romo, F. J. et al. A Crystalline Imine-Linked 3-D Porous Covalent Organic Framework. *J. Am. Chem. Soc.* **131**, 4570-4571 (2009).

7. Sun, Z. et al. Finite phenine nanotubes with periodic vacancy defects. *Science* **363**, 151-155 (2019).
8. Heo, J-M. et al. Chromogenic Tubular Polydiacetylenes from Topochemical Polymerization of Self-Assembled Macrocyclic Diacetylenes. *Macromolecules* **50**, 900-913 (2017).
9. Qiu, C. et al. Scaling carbon nanotube complementary transistors to 5-nm gate lengths, *Science* **355**, 271 (2017).
10. Guo, K. et al. Hierarchical Micro cables Constructed by CoP@C⊂Carbon Framework Intertwined with Carbon Nanotubes for Efficient Lithium Storage. *Adv. Energy Mater.* **10**, 1902913 (2020).
11. Zhou, Y. B. et al. Antimicrobial Nanotubes Consisting of Ag-Embedded Peptidic Lipid-Bilayer Membranes as Delivery Vehicles. *Adv. Mater.* **21**, 1742-1745 (2009).
12. Iijima, S. Helical microtubules of graphitic carbon. *Nature* **354**, 56-58 (1991).
13. Iijima, S., lchihashi, T. Single-shell carbon nanotubes of 1-nm diameter. *Nature* **363**, 603-604 (1993).
14. Bethune, S. D. et al. Cobalt-catalysed growth of carbon nanotubes with single-atomic-layer walls. *Nature* **363**, 605-607 (1993).
15. Dresselhaus, M., Dresselhaus, G. & Avouris, P. (eds) Carbon Nanotubes: Synthesis, Properties and Applications (Springer, 2001).
16. Kato, T. & Hatakeyama, R. Direct growth of short single-walled carbon nanotubes with narrow-chirality distribution by time-programmed plasma chemical vapor deposition. ACS Nano 4, 7395–7400 (2010).
17. Harutyunyan, A. R. et al. Preferential growth of single-walled carbon nanotubes with metallic conductivity. *Science* **326**, 116-120 (2009).

18. Yang, F. et al. Chirality-specific growth of single-walled carbon nanotubes on solid alloy catalysts. *Nature* **510**, 522-524 (2014).
19. Bong, D. T., Clark, T. D., Granja, J. R. & Ghandiri, M. R. Self-assembling organic nanotubes. *Angew. Chem. Int. Ed.* **40**, 988–1011 (2001).
20. Liang, R., A, R., Xu, S., Qi, Q., Zhao, X. Fabricating Organic Nanotubes through Selective Disassembly of Two-Dimensional Covalent Organic Frameworks. *J. Am. Chem. Soc.* **142**, 70–74 (2020).
21. Gong, B., Shao, Z. Self-Assembling Organic Nanotubes with Precisely Defined, Sub-nanometer Pores: Formation and Mass Transport Characteristics. *Acc. Chem. Res.* **46**, 2856–2866 (2013).
22. Murdock, C. R., & Jenkins, D.M. Isostructural Synthesis of Porous Metal–Organic Nanotubes. *J. Am. Chem. Soc.*, **31**, 10983–10988 (2014).
23. Rodríguez-Vázquez, N., Amorína, M., & Granja, J. R. Recent advances in controlling the internal and external properties of self-assembling cyclic peptide nanotubes and dimers. *Org. Biomol. Chem.*,**15**, 4490-4505 (2017).
24. Moreno-Alcántar, G. et al. Solvent- Driven Supramolecular Wrapping of Self-Assembled Structures. *Angew. Chem. Int. Ed.* **60**, 5407-5413 (2021).
25. Datta, S. et al. Self-assembled poly-catenanes from supramolecular toroidal building blocks. *Nature* **583**, 400-405 (2020).
26. Perego, C., Pesce, L., Capelli, R., George, S. J., Pavan, G. M. Multiscale Molecular Modelling of ATP-fueled Supramolecular Polymerisation and Depolymerisation. *Chem. Systems Chem.* **2**, e2000038 (2020).
27. Kumar, S., Rosenberg, J. M., Bouzida, D., Swendsen, R. H., Kollman, P. A., THE weighted histogram analysis method for free- energy calculations on biomolecules. I. *The method. J. Comput. Chem.* **13**, 1011-1021(1992).

28. Pochan, J. D. et al. Toroidal Triblock Copolymer Assemblies. Science, 306, 94-97 (2004).
29. Lee, J. et al. Hollow nano-tubular toroidal polymer microrings. *Nat. Chem.* **6**, 97-103 (2014).
30. Sano, M., Kamino, A., Okamura, J., Shinkai, S. Ring Closure of Carbon Nanotubes. *Science* **293**, 1299-1301 (2001).
31. Martel, R., Shea, H., Avouris, P. Ring Formation in Single-Wall Carbon Nanotubes. *J. Phys. Chem. B* **103**, 36 (1999).

Methods

Synthesis of monomer. In the typical monomer synthesis, *2*-methoxybenzaldehyde (27.2 mg, 0.2 mmol) was taken in dry DCM in the presence of 6 (M) AcOH as the catalyst. Dilute DCM solution of TAT (15.7 mg, 0.05 mmol) was then added to the reaction mixture and stirred for 24 hours. The dry yellow powder was collected after the evaporation of DCM. The powder was dissolved in methanol and characterized by High-Resolution Mass Spectroscopy (HRMS).

Synthesis of CONT-1. *2,5*-dimethoxy-*1,4*-benzene dicarbaldehyde (DMDA) (19.4 mg, 0.1 mmol) was dissolved in 100 mL CH_2Cl_2 (dry, degassed), and 0.5 mL 6 (M) AcOH was added directly into the yellow-colored homogeneous solution as a catalyst of Schiff base reaction. A solution of tetraaminotryptycene (TAT) (15.7 mg, 0.05 mmol) in 50 mL CH_2Cl_2 (dry, degassed) was added dropwise using a dropping funnel with stirring at room temperature under argon atmosphere for 24 hours. The resulting cloudy precipitate was filtered and washed with excess anhydrous methanol. Yield: 25 mg ,78% (calculated with respect to TAT).

Synthesis of CONT-2. Terephthalaldehyde (TA) (13.4 mg, 0.1 mmol) was dissolved in 100 mL dry degassed Dichloromethane (DCM), and 0.5 mL 6 (M) AcOH was added directly into

solution as a catalyst of Schiff base reaction. A solution of tetraaminotryptycene (TAT) (15.7 mg, 0.05 mmol) in 50 mL dry DCM was added dropwise using a dropping funnel with stirring at room temperature under Argon atmosphere for 24 hours. The resulting cloudy precipitate was filtered and washed with excess anhydrous methanol. Yield: 13.3 mg, 51% (calculated with respect to TAT).

Synthesis of toroid. 2 mg intertwined CONT-1 was taken in 50 mL anhydrous THF and sonicated at room temperature for 20 mins. The nanotubes are transformed into toroids. The as-synthesized toroids are separated from mixture with intertwine nanotubes by simple filtration technique with Whatman 42 filter paper (Pore size 2 μm).

Computational Methods

All simulations were performed with the GROMACS 2018 software[32,33] equipped with PLUMED2.5[34,35] (for the umbrella sampling simulations and systems analysis). The AA CONT-1 model was parameterized based on the General Amber Force-Field (GAFF),[36] setting the partial charges *via* the Restrained Electrostatic Potential and using PM6 and Hartree-Fock (with the 6-31g* basis set) levels of theory[37] for geometry optimization. The organic solvent molecules (DCM and THF) were parametrized compatibly with the GAFF, and the TIP3P model was used for water.[38] The CG CONT model was constructed to fit with the AA one.[39] Details on the modeling and on the setup of the AA-MD and CG-MD simulations are reported in the Supplementary Information.

32. Berendsen, H. J. C., van der Spoel, D., van Drunen, R. GROMACS: A message-passing parallel molecular dynamics implementation. *Comput. Phys. Commun.* **91**, 43–56 (1995).
33. Abraham, M. J. et al. GROMACS: High performance molecular simulations through multi- level parallelism from laptops to supercomputers. *SoftwareX* **1**, 19–25 (2015).
34. Tribello, G. A., Bonomi, M., Branduardi, D., Camilloni, C., Bussi, G. PLUMED 2: New feathers for an old bird. *Comput. Phys. Commun.* **185**, 604–613 (2014).

35. The PLUMED Consortium, Promoting transparency and reproducibility in enhanced molecular simulations. *Nat. Methods.* **16**, 670–673 (2019).
36. Wang, J., Wolf, R. M., Caldwell, J. W., Kollman, P. A., Case, D. A. Development and testing of a general amber force field. *J. Comput. Chem.* **25**, 1157–1174 (2004).
37. Bayly, C. I., Cieplak, P., Cornell, W., Kollman, P. A. A well-behaved electrostatic potential based method using charge restraints for deriving atomic charges: the RESP model. *J. Phys. Chem.* **97**, 10269–10280 (1993).
38. Jorgensen, W. L., Chandrasekhar, J., Madura, J. D., Impey, R. W., Klein, M. L. Comparison of simple potential functions for simulating liquid water. *J. Chem. Phys.* **79**, 926–935 (1983).
39. Empereur-Mot, C. et al. Swarm-CG: Automatic Parametrization of Bonded Terms in MARTINI-Based Coarse-Grained Models of Simple to Complex Molecules *via* Fuzzy Self-Tuning Particle Swarm Optimization. *ACS Omega* **5**, 32823–32843 (2020).
40. Leanza, L., Perego, C., Pesce, L., Capelli, R., and Pavan, G.M. Computational Data supporting " Porous covalent organic nanotubes and their assembly in loops and toroids", Zenodo, 10.5281/zenodo.5769788, 2022.

Data availability

All data supporting the findings of this study, including synthesis, experimental procedures, and compound characterization, are available within the Article and its Supplementary Information. Structure and parameter files for the AA and CG models of the CONT-1 tubules used in the simulations are available at https://doi.org/10.5281/zenodo.5769788 (ref. 40) Supplementary Information is available in the online version of the paper. Reprints and permissions information is available online at www.nature.com/reprints. Correspondence and requests for materials should be addressed to R.B.

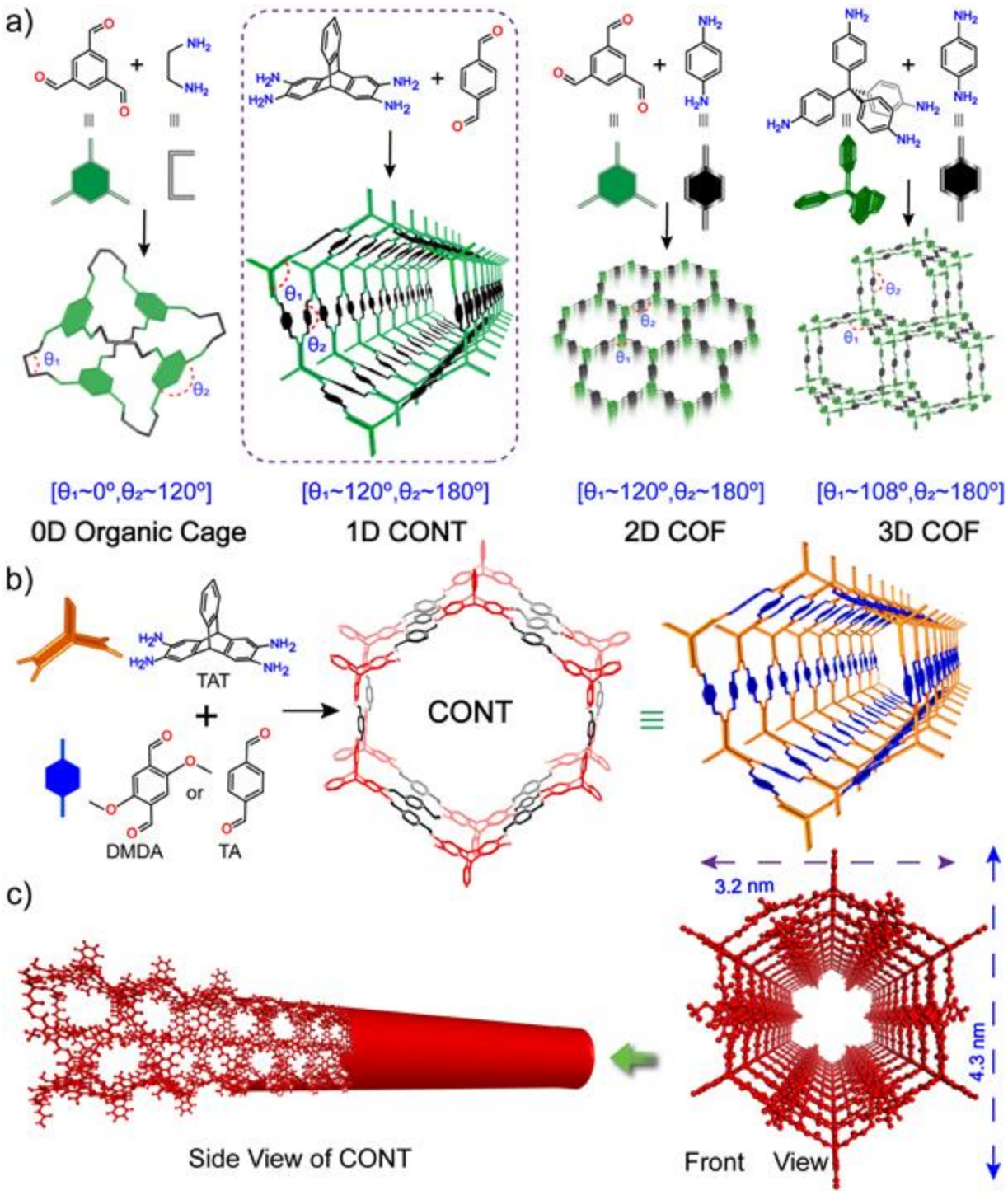
a)
[θ1~0°,θ2~120°]
0D Organic Cage
[θ1~120°,θ2~180°]
1D CONT
[θ1~120°,θ2~180°]
2D COF
[θ1~108°,θ2~180°]
3D COF
b)
TAT
DMDA
or
TA
CONT
c)
3.2 nm
4.3 nm
Side View of CONT
Front View

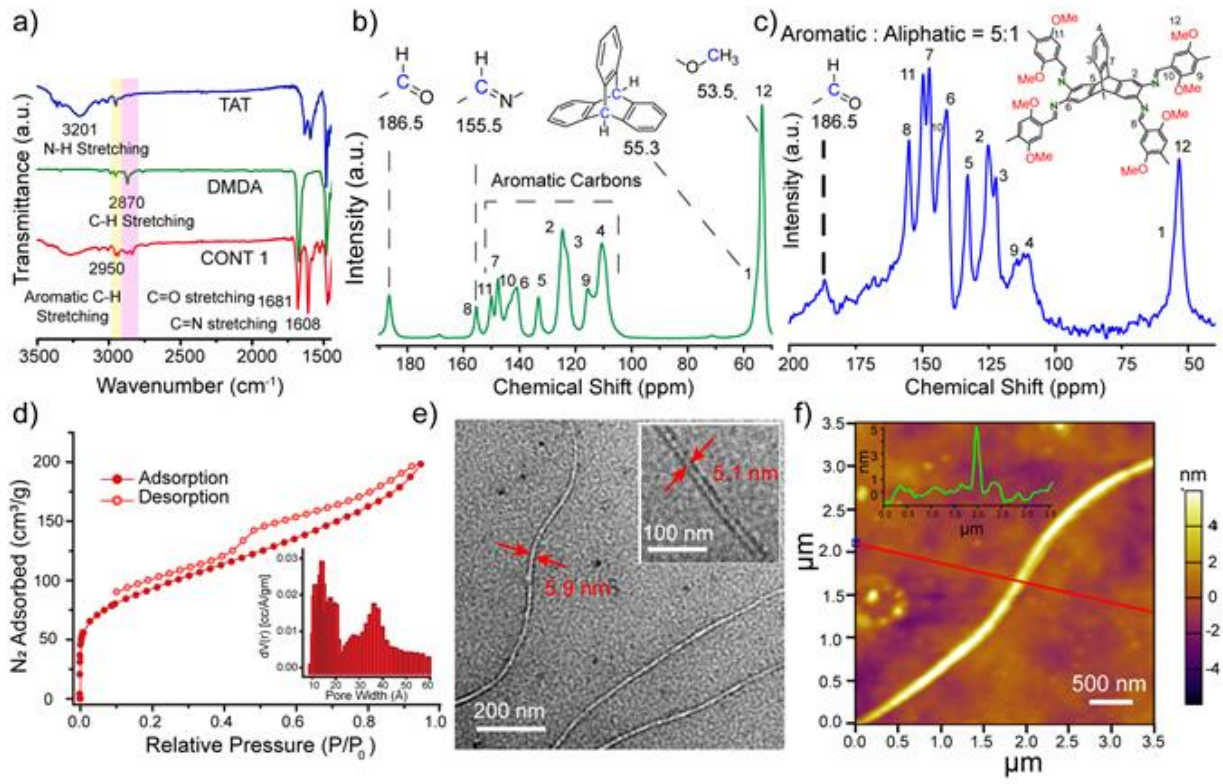
a)
TAT
DMDA
CONT 1
3201
N-H Stretching
2870
C-H Stretching
2950
Aromatic C-H
Stretching
C=O stretching 1681
C=N stretching 1608
Transmittance (a.u.)
Wavenumber (cm-1)
b)
186.5
155.5
55.3
53.5
Aromatic Carbons
Intensity (a.u.)
Chemical Shift (ppm)
c)
Aromatic : Aliphatic = 5:1
186.5
Intensity (a.u.)
Chemical Shift (ppm)
d)
Adsorption
Desorption
N2 Adsorbed (cm3/g)
Relative Pressure (P/P0)
dV(r) [cc/Å/g]
Pore Width (Å)
e)
5.1 nm
100 nm
5.9 nm
200 nm
f)
500 nm
µm
nm

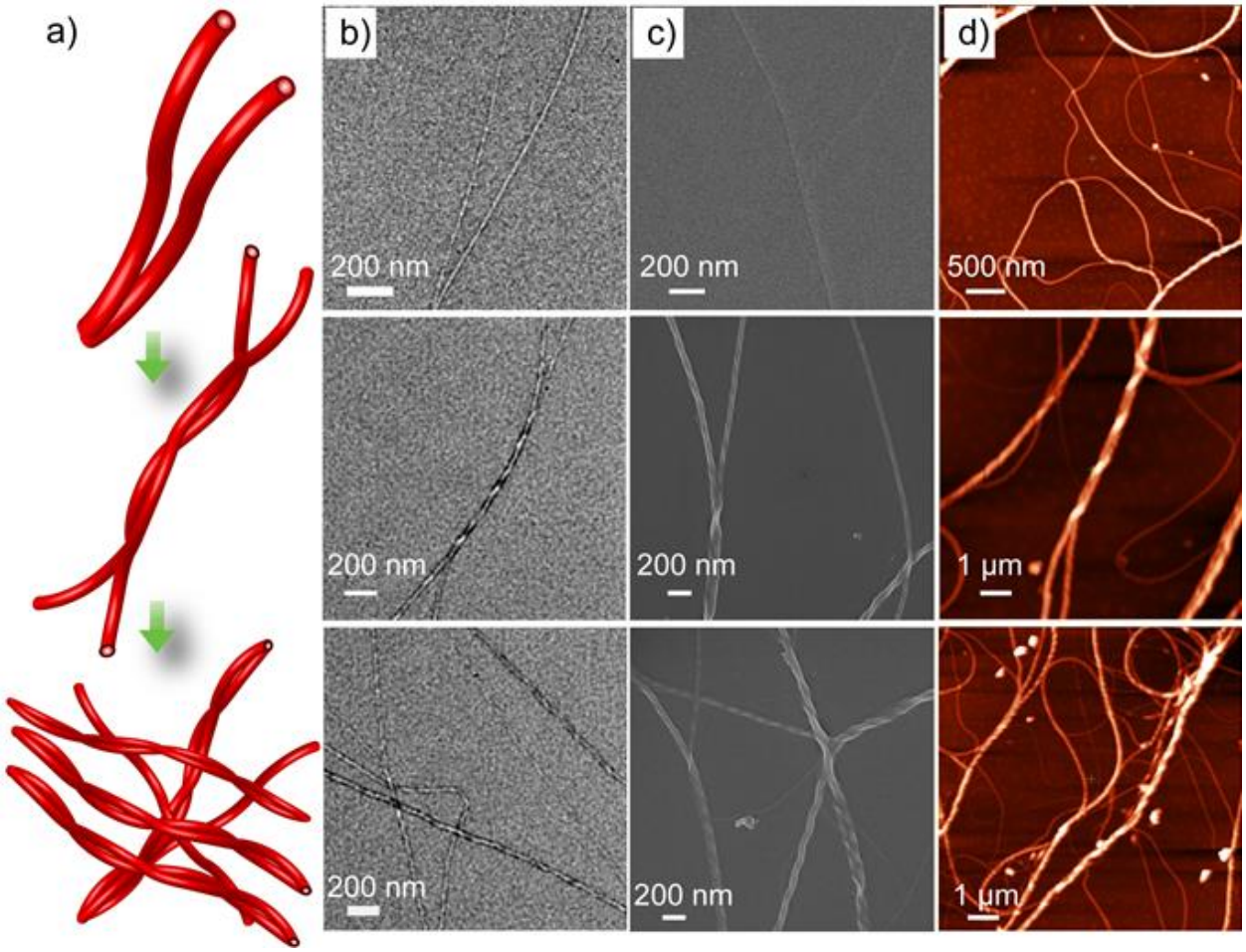
a)
b)
c)
d)
200 nm
200 nm
500 nm
200 nm
200 nm
1 µm
200 nm
200 nm
1 µm

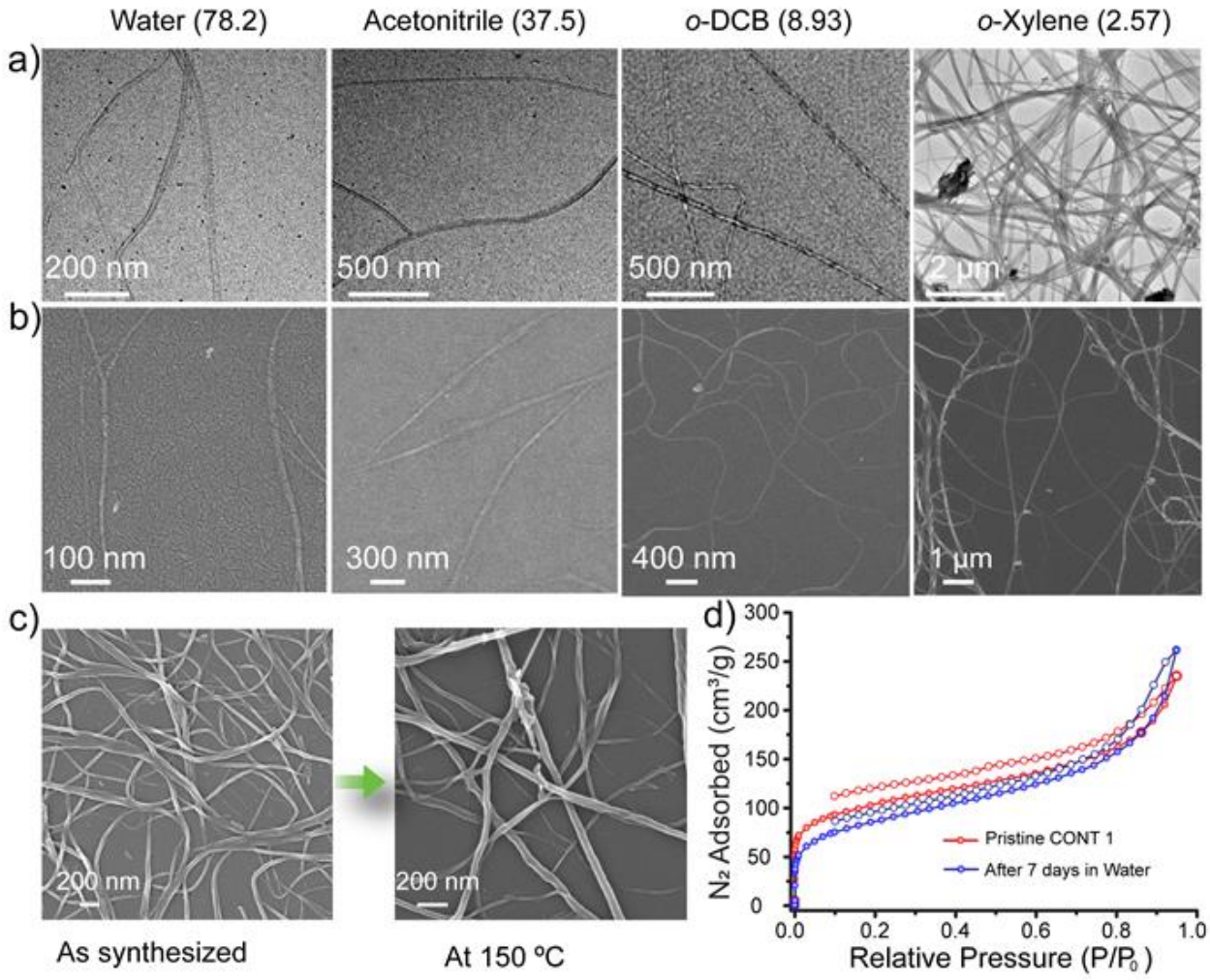
Water (78.2)
Acetonitrile (37.5)
o-DCB (8.93)
o-Xylene (2.57)
a)
200 nm
500 nm
500 nm
2 μm
b)
100 nm
300 nm
400 nm
1 μm
c)
200 nm
200 nm
As synthesized
At 150 °C
d)
N2 Adsorbed (cm3/g)
Relative Pressure (P/P0)
Pristine CONT 1
After 7 days in Water
0
50
100
150
200
250
300
0.0
0.2
0.4
0.6
0.8
1.0

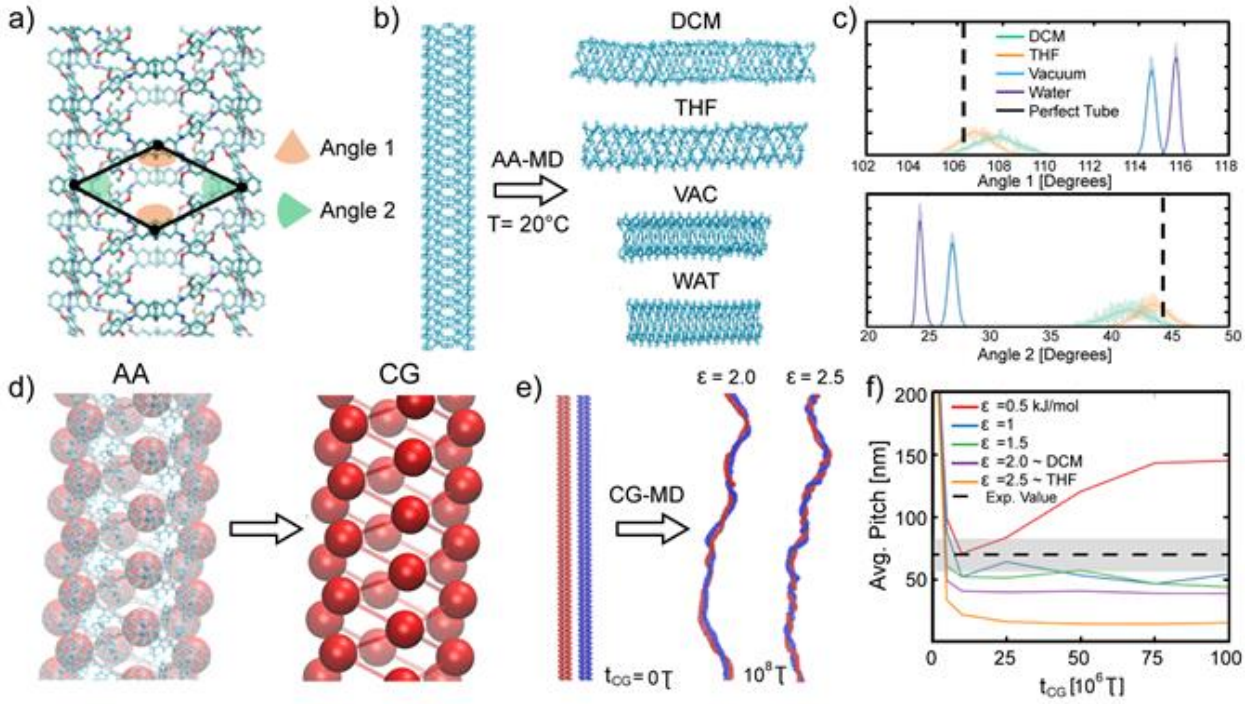
a)
Angle 1
Angle 2
b)
AA-MD
T= 20°C
DCM
THF
VAC
WAT
c)
DCM
THF
Vacuum
Water
Perfect Tube
Angle 1 [Degrees]
Angle 2 [Degrees]
d)
AA
CG
e)
CG-MD
ε = 2.0
ε = 2.5
t_{CG}= 0 τ
10^8 τ
f)
ε =0.5 kJ/mol
ε =1
ε =1.5
ε =2.0 ~ DCM
ε =2.5 ~ THF
Exp. Value
Avg. Pitch [nm]
t_{CG} [10^6 τ]

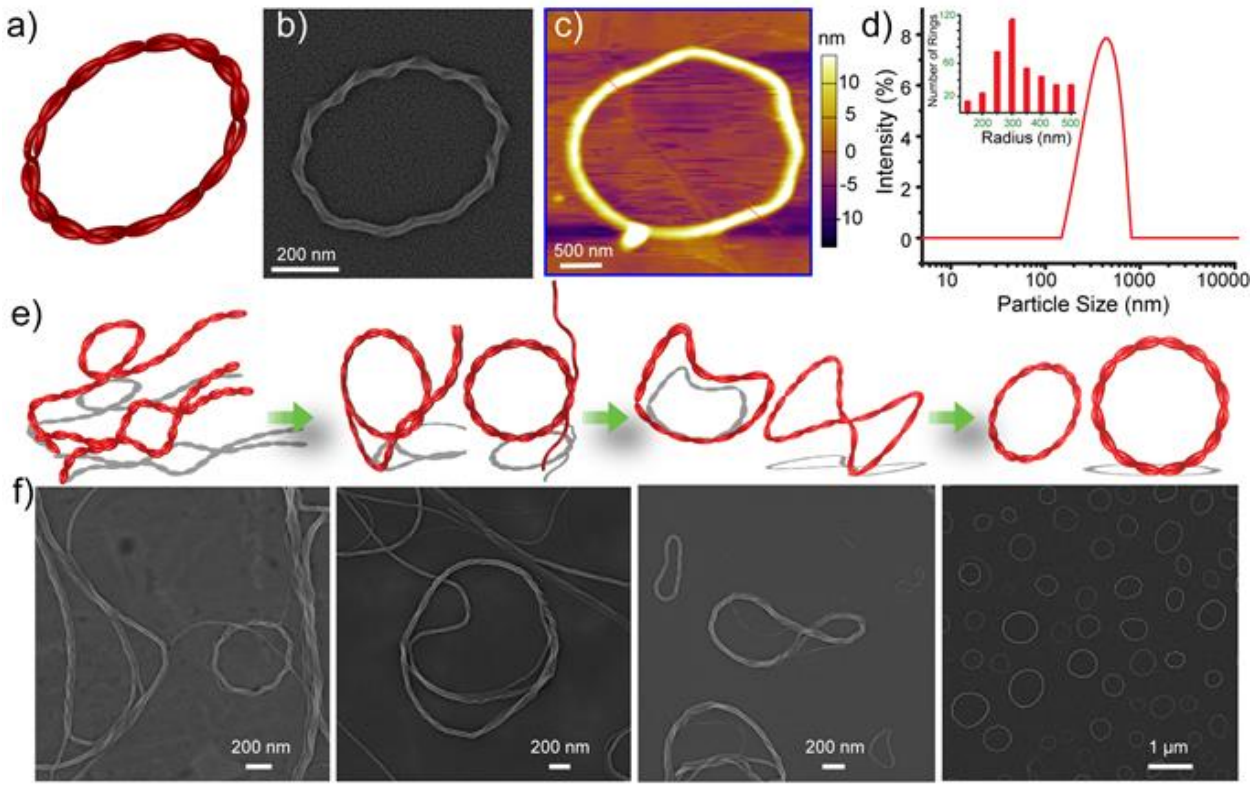
a)
b)
200 nm
c)
500 nm
nm
10
5
0
-5
-10
d)
Intensity (%)
Particle Size (nm)
Number of Rings
Radius (nm)
e)
f)
200 nm
200 nm
200 nm
1 µm

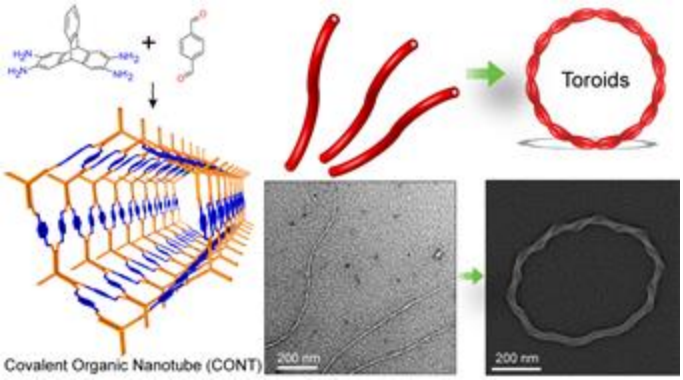
Toroids
Covalent Organic Nanotube (CONT)
200 nm
200 nm